Luo, W., Xiong, C., Zhu, Z., Mei, X. (2018): Onset Condition of Plasma Density Enhancements: A Case Study for the Effects of Meridional Wind During 17-18 August 2003. - *Journal of Geophysical Research*, *123*, 8, pp. 6714—6726.

DOI: http://doi.org/10.1029/2018JA025191

Journal of Geophysical Research: Space Physics

RESEARCH ARTICLE
10.1029/2018JA025191

Key Points:
- The plasma depletions and enhancements were observed by ROCSAT-1 at different local time before midnight on 17 August 2003
- The EIA displayed different characteristics during 17–18 August 2003 from CHAMP, GRACE, and TEC map, respectively
- The effects of the meridional wind on the formation of plasma blobs are discussed

Correspondence to:
W. Luo,
whlu@whu.edu.cn

Citation:
Luo, W., Xiong, C., Zhu, Z., & Mei, X. (2018). Onset condition of plasma density enhancements: A case study for the effects of meridional wind during 17–18 August 2003. *Journal of Geophysical Research: Space Physics*, *123*, 6714–6726. https://doi.org/10.1029/2018JA025191

Received 3 JAN 2018
Accepted 11 JUL 2018
Accepted article online 16 JUL 2018
Published online 4 AUG 2018

Onset Condition of Plasma Density Enhancements: A Case Study for the Effects of Meridional Wind During 17–18 August 2003

Weihua Luo[1,2], Chao Xiong[3], Zhengping Zhu[1,2], and Xuefei Mei[4]

[1]College of Electronic and Information Engineer, South-Central University for Nationalities, Wuhan, China, [2]Hubei Key Laboratory of Intelligent Wireless Communications, South-Central University for Nationalities, Wuhan, China, [3]Helmholtz Centre Potsdam, GFZ German Research Centre for Geosciences, Potsdam, Germany, [4]School of Electronic Information, Wuhan University, Wuhan, China

Abstract The multisatellite observations were used to study the possible factors leading to the development of the plasma density enhancements during the August 2003 storm period. The plasma depletions and enhancements (also referred as bubbles and blobs, respectively) were observed by first satellite of the Republic of China around 345°E sector at different local time on 17 August, before the midnight after the storm sudden commencement. However, only the depletions were recorded on 18 August at the same longitude sector and at nearly the same time as that on 17 August. The motions of the bubbles and blobs displayed different characteristics on 17 August. From Challenging Mini-satellite Payload, Gravity Recovery and Climate Experiment, and total electron content map, the equatorial ionization anomaly was inhibited and displayed more asymmetric on 17 August and became stronger on 18 August. A density enhancement near the northern crest was recorded by Gravity Recovery and Climate Experiment, and similar enhancements were found in total electron content map at low-latitude regions of both hemispheres on 17 August. The results suggest that the meridional neutral wind is crucial and plays an important role in the development of the plasma blobs. And the variations of meridional neutral wind may be linked with the large-scale traveling ionospheric disturbances during the disturbed periods.

1. Introduction

Since the plasma density enhancements (blobs) in low-latitude ionosphere were first reported by Oya et al. (1986) and Watanabe and Oya (1986), the characteristics of plasma blobs have been widely investigated from satellites and nightglow images (Huang et al., 2014; Kil et al., 2011, 2015; Le et al., 2003; Park et al., 2008; Pimenta et al., 2004, 2007). For example, the blobs are usually detected around ±20° magnetic latitudinal regions (Choi et al., 2012; Watanabe & Oya, 1986). The occurrence of blobs has a complementary nature with that of the equatorial and low-latitudinal plasma depletions (bubbles) and is not affected by the solar activity and geomagnetic activity (Park et al., 2003; Watanabe & Oya, 1986), and there is some similarity in the seasonal-longitudinal distributions of blobs and bubbles (Park et al., 2003, 2008). The mechanism leading to the formation of the blob has not been completely understood yet. Based on the observations from Communication/Navigation Outage Forecasting System satellite during solar minimum, Haaser et al. (2012) suggested that there may exist several types of plasma blobs driven by different mechanisms. Some studies have shown that the occurrence of blob may be linked with the plasma bubbles in equatorial region (e.g., Huang et al., 2014; Le et al., 2003; Martinis et al., 2009; Yokoyama et al., 2007), and the model simulations also showed that the blob could occur as a consequence of the development of bubbles (Krall et al., 2010). Thus, it is suggested that the blob related with the bubbles may be formed due to the eastward polarization electric field (Huang et al., 2014; Le et al., 2003). Other studies show that the blob may be an independent phenomena and is linked with other factors, such as medium-scale traveling ionospheric disturbances (MSTIDs; Kil et al., 2015; Martinis et al., 2009). Some authors also proposed that the meridional neutral wind may be related with the occurrence of blobs (Krall, Huba, & Martinis, 2009; Martinis et al., 2009; Park et al., 2003), without providing enough evidences. Therefore, the factors linked with the formation of blobs are necessary to be further studied.

In this case study, observations from multisatellites, including satellite of the Republic of China (ROCSAT-1), Challenging Mini-satellite Payload (CHAMP), and Gravity Recovery and Climate Experiment (GRACE), and

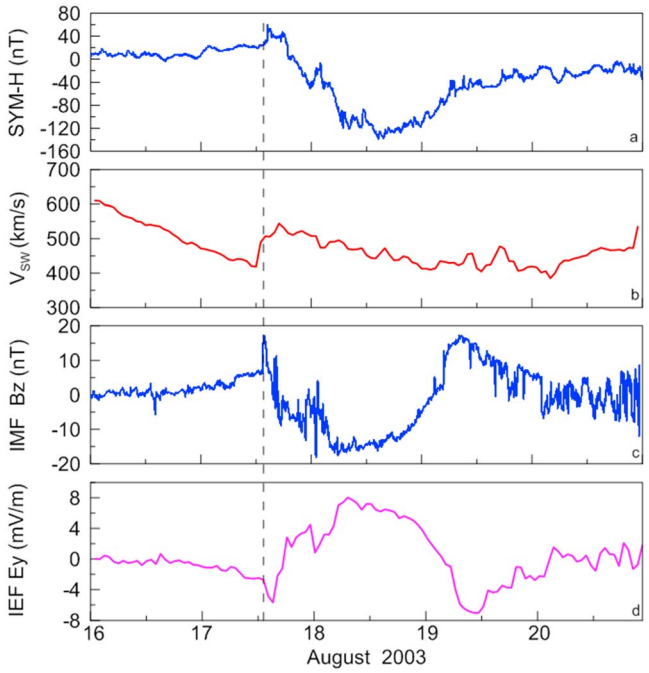

Figure 1. (a) The SYM-H index, (b) solar wind speed V_{SW}, (c) interplanetary magnetic field B_z component, and (d) interplanetary electric field E_y from 16 to 20 August 2003.

the total electron content (TEC) map from International GNSS Service (IGS) are used to study the low-latitude ionospheric variations in 345°E sector and the possible factors leading to the development of the plasma blobs during 17–18 August 2003.

2. Data Description and Geophysical Conditions

The ROCSAT-1 was launched on March 1999 to a circular orbit with a 35° inclination orbital plane at 600 km and a period of 97 min. The onboard Ionospheric and Plasma Electrodynamics Instrument operates at 100% duty cycle to take continuous data of ion density and ion composition in the low-to-middle latitude ionosphere(Yeh et al., 1999). The planar Langmuir probe on board the CHAMP satellite was used to measure the in situ electron density and temperature per 15 s; the planar Langmuir probe electron density measurements have been validated by comparison with digisonde measurements at Jicamarca, which were consistent with that from the digisonde (McNamara et al., 2007). The GRACE mission was launched on 17 March 2002 into a near-circular, polar orbit (inclination: 89°). The altitude of the satellites is quite stable over the years, and now it stays around 480 km (Tapley et al., 2004). The derived electron density has been validated by ground based radars of European Incoherent Scatter radar, Millstone hill, and Arecibo (Xiong et al., 2015), and the more detailed description of the electron density retrieval can be found in Xiong et al. (2010).

SYM-H index, interplanetary parameters during the storm period including solar wind speed (V_{sw}), the component of interplanetary magnetic field (IMF) B_z, and the derived interplanetary electric field (IEF) E_y are displayed in Figure 1.

The Storm Sudden Commencement (SSC) of the geomagnetic storm during 17–20 August 2003 occurred at 1421 universal time (UT) on 17 August; the SYM-H index achieved a minimum about −148 nT around 1600 UT on 18 August. The *Bz* component was southward since the main phase till about 0200 UT on August 19. The V_{sw} started to increase about 1200 UT of 17 August, from about 440 to 540 km/s, and it remained during the main phase and recovery phase of the storm. After the storm started, E_y was westward and turned to eastward from about 1800 UT of 17 to 18 August , with a maximum value of about 8 mV/m.

3. Observations

3.1. ROCSAT-1 Observations

Figure 2 displays the ion density, three components of ion velocity, ion compostion, and ion temperature from ROCSAT-1 in 345°E region during 22.5 UT-22.6 UT on 17 August (I) and from 0.29 UT to 0.4 UT on 18 August (II) 2003, respectively. $V_{meridional}$ and V_{zonal} are the two components perpendicular to the field line in the meridional (upward) and zonal (eastward) direction, respectively. $V_{parallel}$ is the field-aligned component. Dip latitude, geographic longitude, UT, and local time (LT) are noted at the bottom of figure.

It can be seen from Figure 2 that two bubbles were detected in equatorial region. At 1.85°N, the plasma density was about 1.68×10^4 cm^{-3} around 343°E, and the background plasma density was about 3.07×10^5 cm^{-3}. The depletion was about 94.5%, which was recorded at about 22.59 UT (21.49 LT). At about −0.75°N, the plasma density was 8.32×10^4 cm^{-3}. In the 345°E sector, the depletion was about 72.9%, which was recorded at about 22.6 UT (21.68 LT).

Two blobs were detected in low-latitude region and at the same longitudinal sector several hours after the bubbles were recorded during the main phase of the storm. One located in −20°N region, the background electron density was about 5.47×10^4 cm^{-3}, while the density inside the blob (−20.92°N) was about 2.13×10^5 cm^{-3}, the enhancement was about 289.9%, which occurred at 0.35 UT (LT was about 23.38 LT on 17 August). The region of the enhancement was from −21.29°N to −19.39°N, which means the scale

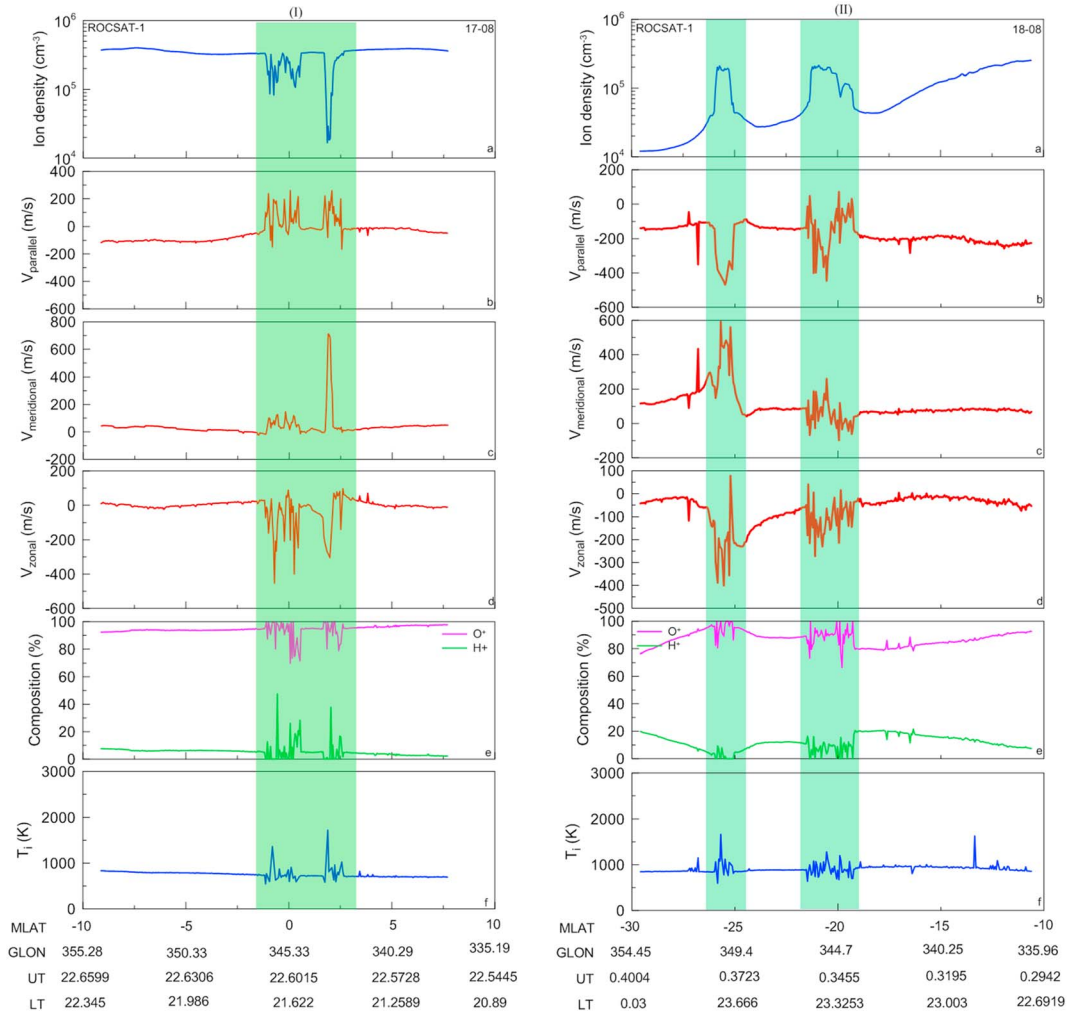

Figure 2. The ion density, drift, composition, and temperature observed from ROCSAT-1 in 345°E sector during 22.5–22.6 UT on 17 August 2003 (I) and during 0.29–0.4 UT on 18 August 2003 (II), respectively. $V_{parallel}$ is the field-aligned component, $V_{meridional}$ is meridional, V_{zonal} is zonal. Satellite altitudes were 588.2 km (I) and 584.6 km (II), respectively.

in latitude was about 1.9°. The other was around −25°N, the background electron density was about 5.74×10^4 cm^{-3}, while the density inside the blob (−25.73°N) was about 2.09×10^5 cm^{-3}, and the enhancement was about 264.8% from −25.94°N to −25.22°N, which was recorded at 0.376 UT (LT was 23.71 LT on 17 August).

In Figure 2, it can be noticed that the motions of the bubbles and blobs were different along the field lines. Inside the plasma bubbles, the plasma turned to move northward, while the background plasma moved southward. Inside and outside the plasma blobs, shown in Figure 2II, the plasma moved southward and the plasma velocity inside the blobs increased sharply and exceeded 400 m/s.

Figure 3 displays the ion density, three components of ion velocity, ion compostion, and ion temperature from ROCSAT-1 in 345°E region from 22.5 UT to 22.7 UT on 18 August 2003 (I) and during 0.29–0.4 UT on 19 August 2003 (II), respectively. The data formats are the same as that in Figure 2.

In 2.34–3.01°N region, shown in Figure 3I, the plasma density decreased to 6.17×10^4 cm^{-3} around 336.3°E on 18 August, where the background plasma density was about 5.07×10^5 cm^{-3}. The depletion was about 87.8%, which was recorded at about 22.64 UT (21.07 LT). At about −10°N, the plasma density could decrease to 2.59×10^5 cm^{-3} in 348°E, and the depletion was about 61.5%, which was recorded at about 22.7 UT (21.97 LT).

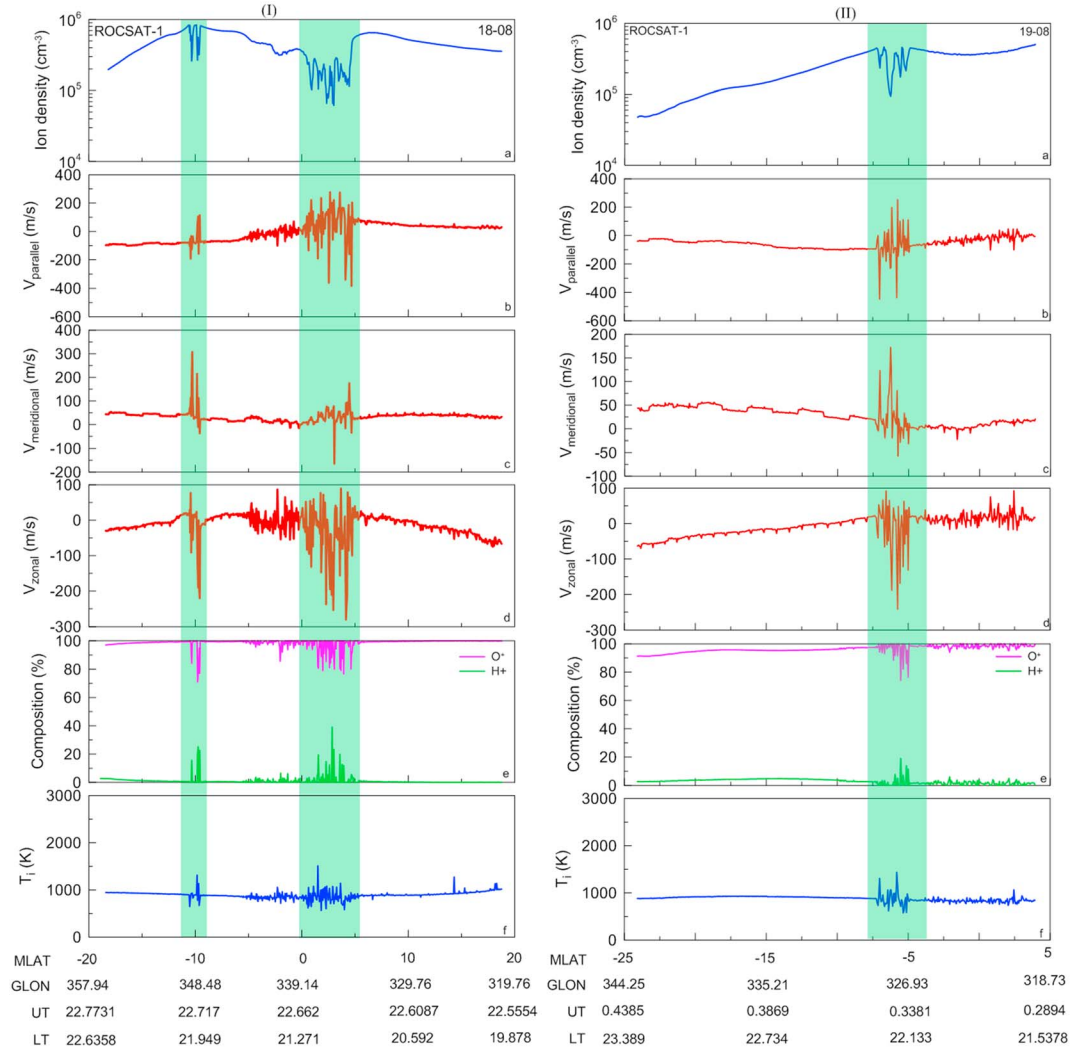

Figure 3. The ion density, drift, composition, and temperature observed from ROCSAT-1 in 345°E sector during 22.55–22.77 UT on 18 August 2003 (I) and during 0.29–0.4 UT on 19 August 2003 (II), respectively. The formats are the same as in Figure 2. Satellite altitudes were 593.5 km (I) and 589.4 km (II), respectively.

As shown in Figure 3II, around −6.27°N, a plasma bubble was also detected in 327°E at 0.34 UT on 19 August 2003 (LT was 22.2 LT on 18 August). The depletion inside the bubble was about 72.7%. The density was about 9.42×10^4 cm^{-3}, and the background density was about 3.45×10^5 cm^{-3}. There were no other plasma depletions or enhancements in 345°E sector recorded by the satellite.

Comparing Figure 3 with Figure 2, the depletions in different latitudinal regions were recorded by the satellite at nearly the same time on 17 and 18 August, respectively.

3.2. CHAMP and GRACE Observations

Figure 4 displays the plasma densities in 345°E sector at lower altitudes from CHAMP (400 km) and GRACE(480 km) on 17 and 18 August 2003, respectively.

The strength (crest-to-trough ratio, CTR) and density asymmetry (ASY) of EIA are calculated as CTR = (N + S/2T), ASY = (N − S)/(N + S), which are shown in Figure 4, respectively. N(S) represents the density above the northern (southern) crest, while T represents the density above the trough.

It can be seen from Figure 4 that the EIA was inhibited on 17 August 2003 and became stronger on 18 August at both GRACE and CHAMP altitudes. On 17 August, the density above the crests and EIA strength was smaller than that on 18 August, while EIA ASY was more remarkable.

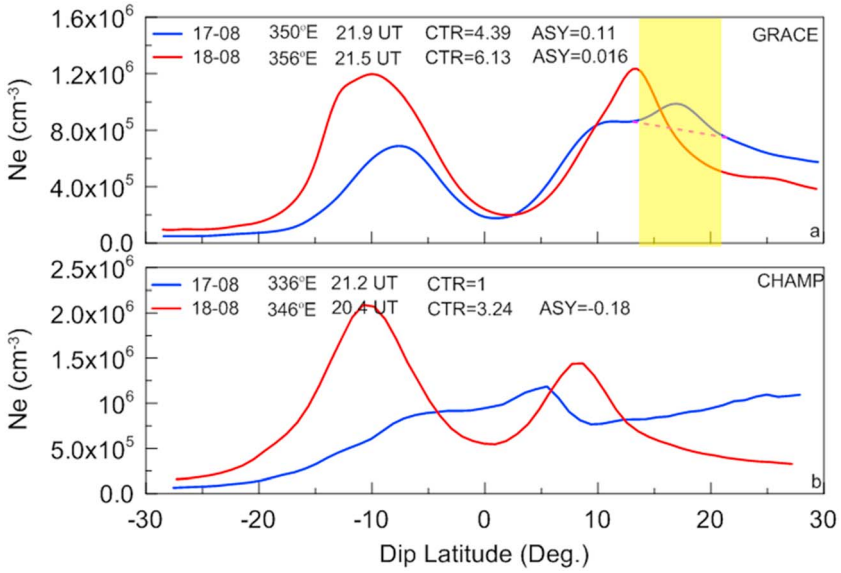

Figure 4. Electron density from (a) Gravity Recovery and Climate Experiment and (b) Challenging Mini-satellite Payload in 345°E region during 17–18 August 2003. The interplanetary electric field strength and density asymmetry indices are marked in the figures, respectively. The yellow shade represents the density enhancement.

At GRACE altitude, the densities above the crests were about 1.2×10^6 cm^{-3} (at −10.1°N) and 1.23×10^6 cm^{-3} (at 13.5°N) on 18 August, respectively. The densities above the crests were about 6.89×10^5 cm^{-3} (at −7.6°N) and 8.63×10^5 cm^{-3} (at 11.2°N) on 17 August, respectively. It should be noticed that a density enhancement was recorded at 21.97 UT at 16.95°N, noted by the yellow shade in the figure, which was about 14.9% with respect to the background.

At CHAMP altitude, the densities above the crests were about 2.09×10^6 cm^{-3}and 1.44×10^6 cm^{-3}on 18 August, respectively. The density above the trough was about 1.19×10^6 cm^{-3} around 7.54°N on 17 August, which was smaller obviously than that on 18 August.

3.3. TEC Variations

Figure 5 presents the IGS TEC map with UTs in 345°E sector during 16–18 August 2003. The dip equator is noted as the dashed line in the figure.

Figure 5 shows quite different patterns of EIA during the three days. The TEC decreased on 17 August with respect to that on 16 August and displayed increases on 18 August, especially after 2000 UT. The EIA displayed remarkable asymmetric on 17 August. The northern EIA crest moved farther away from the dip equator, while the southern crest located much closer to the equator. The EIA crests on 18 August located closer to the dip equator relative to that on 17 August.

It also should be noted that there were TEC enhancements after 2100 UT in low-latitudinal regions of both hemispheres on 17 August, noted as the magenta circled regions. In southern hemisphere, the enhancements could persist into the midnight of 18 August. Around geographic 27°N, TEC reached about 35 TECU around 2100 UT on 17 August, while the TEC values were less than 20 TECU on 16 and 18 August. Around geographic −5 to −8°N regions, TEC increased to about 28 TECU from 2200 UT of 17 August to 0300 UT of 18 August, while the TEC values were about17 TECU during other two days. As indicated by Dashora and Pandey (2005), the low-latitude TEC enhancements may be related with the plasma blobs recorded by the satellites.

4. Discussion

From the observations of CHAMP and GRACE, it can be noticed that EIA was weaker on 17 August and stronger on 18 August, and the performance of EIA was different at different altitudes. At CHAMP altitude, the EIA

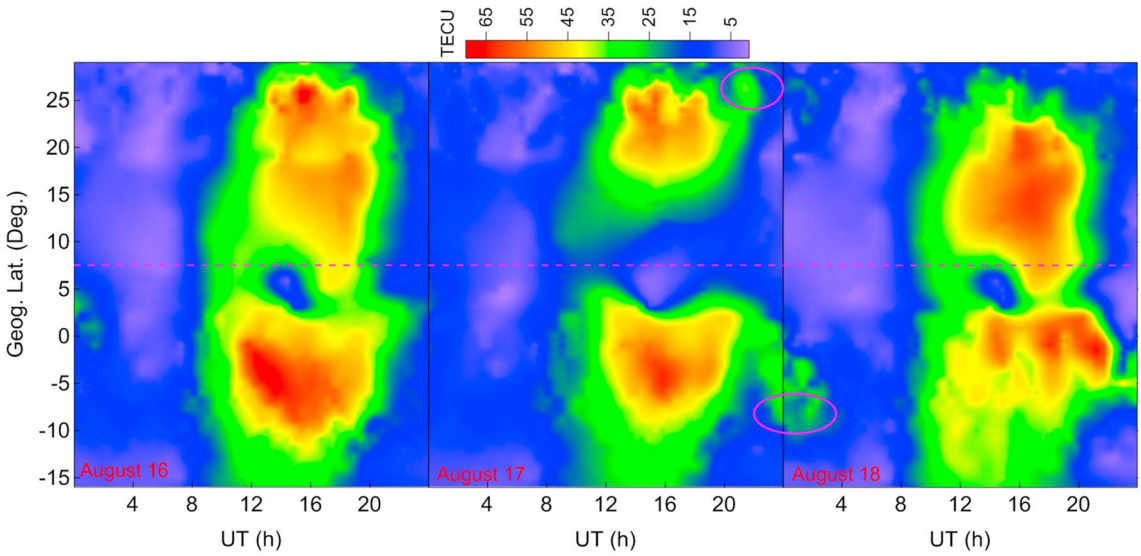

Figure 5. Low-latitude ionospheric total electron content map in 345°E sector from International GNSS Service during 16–18 August 2003. The dashed line represents the dip equator.

was not well developed on 17 August and displayed remarkable asymmetry on 18 August relative to that at GRACE altitude. At GRACE altitude, the CTR was about 6.13 and the ASY was 0.016 on 18 August, while the values were about 4.39 and 0.11 on 17 August, respectively. The performance of EIA at different altitudes means that the EIA became stronger and more symmetric on 18 August. On 18 August, the EIA strength was weaker and asymmetry was more remarkable at lower altitude (CHAMP altitude) relative to that at higher altitude (GRACE altitude).

As shown in Figure 1, the IEF E_y was westward and turned eastward around 1800 UT, with the amplitude of 1–2 mV/m; the inhibition of EIA may not be related with the IEF. As pointed out by some studies, the meridional wind could enhance or inhibit the EIA (Balan et al., 2018; Lin et al., 2005). And the meridional wind is the major factor leading to the asymmetry of EIA (e.g., Aydogdu, 1988; Walker, 1981). Therefore, we assume the variations during 17–18 August, between different altitudes may be attributed to the meridional wind. The existence of poleward meridional wind on 17 August at CHAMP and GRACE altitudes can be concluded. On 18 August, the effect of neutral wind at CHAMP altitude was more remarkable than that at GRACE altitude.

The TEC variations in EIA regions shown in Figure 5 also indicated that there would be the existence of meridional wind on 17 August. On 17 August, the TEC values above the two crests decreased and the EIA showed significant asymmetric, and the EIA displayed much symmetric on 18 August. For instance, on 17 August, TEC above the southern crest was about 62 TECU and about 56 TECU above the northern crest. On 16 August, TECs above the southern and northern crests were about 67 and 72 TECU, respectively. Moreover, on 17 August, TEC map also showed that EIA crests moved farther away from the dip equator with respect to those on 16 and 18 August, and the southern EIA crest was closer to the equator relative to the northern crest, which means that the effects of the poleward meridional winds were remarkable and the winds were interhemispheric asymmetric.

On 18 August, the EIA became stronger and was possibly related to the prompt penetration electric field. As seen from Figure 4, EIA strength was stronger and the crests moved farther away from the dip equator at higher altitude (GRACE), which means that the fountain effect was enhanced. The IEF E_y shown in Figure 1 reached a maximum about 8 mV/m around 1000 UT, leading to the enhancement of fountain effect due to the enhancement of background ionospheric electric field.

Moreover, the existence of meridional wind which may vary with the LTs also affected the occurrences of the plasma bubbles. In Figure 4, the EIA was not well developed around 21 UT (19.6 LT) and formed at about 21.9 UT (21.3 LT) on 17 August, which means that the meridional wind became weaker during the period. As indicated by the previous reports, the meridional wind would suppress the occurrence of the plasma

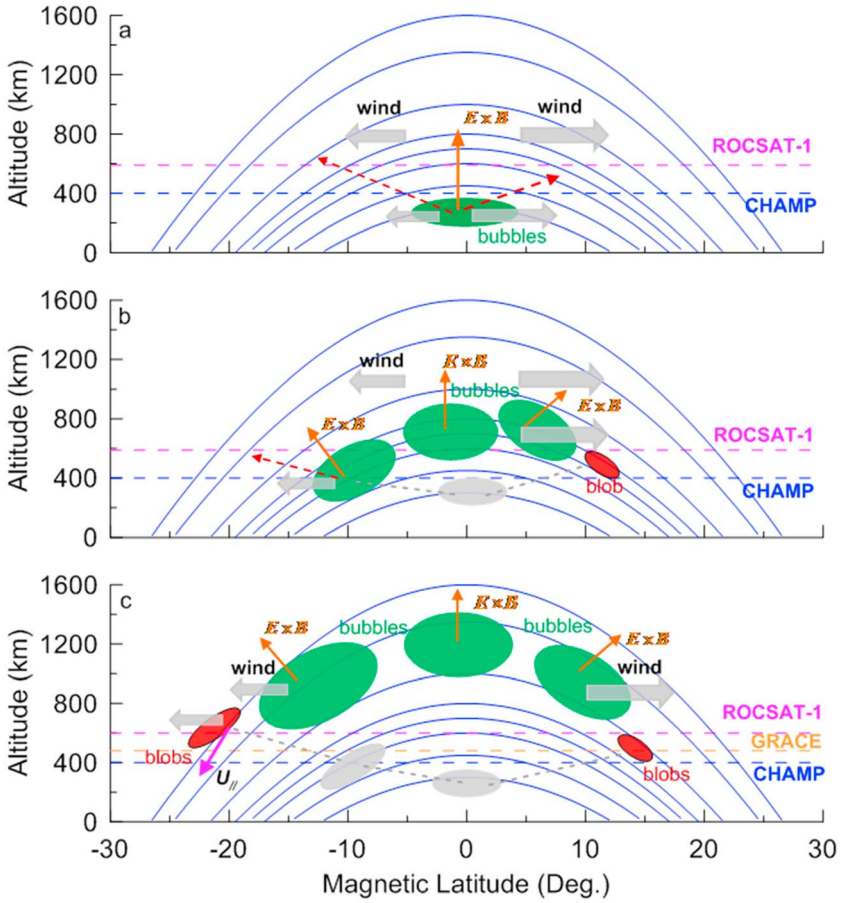

Figure 6. Schematic illustration of the development of plasma density depletions and enhancements, similar with the hypothesis of Huang et al. (2014), under the effects of the zonal polarization electric field and poleward neutral wind. The blue lines represent the geomagnetic field lines. The red blocks represent the plasma density enhancements. The green blocks represent the plasma density depletions. (a) Early stage, (b) intermediate stage, and (c) later stage of the development of the blobs and bubbles. The gray arrows represent the meridional wind, while the longer length represents the stronger wind. The magenta arrow represents the parallel component of the wind ($U_{//}$). The orange arrows represent the upward $E \times B$ drift. The read dashed lines represent the directions of the movement of the particles. The gray dashed lines and the gray blocks represent the trace of the particles and bubbles, respectively.

bubbles (Krall, Huba, Joyce, et al., 2009; Maruyama, 1988; Maruyama et al., 2009). Due to the weakness of the meridional wind, the plasma bubbles were initiated and developed subsequently, as shown in Figure 2l.

As shown in Figures 2 and 3, the plasma blobs and depletions were recorded before the midnight by ROCSAT-1 in same longitudinal sector on 17 August, after the SSC of the storm, while only the depletions were recorded on 18 August at the nearly same time as that on 17 August. These bubbles and blobs displayed some similarities and also some differences. From Figure 2, it can be noted that the motions of the bubbles and blobs were different on 17 August. The movements of blobs and bubbles in meridional and zonal directions were consistent, which were downward and westward, respectively. But the plasma inside the blobs moved southward and the plasma inside the bubbles in equatorial region moved northward.

Comparing Figure 3 with Figure 2, the characteristics of the bubbles on the two days also showed differences. The bubbles expanded to low latitudinal region (about −10°N) on 18 August, while the bubbles that occurred on 17 August were observed in equatorial region. The depletion on 17 August displayed more significantly, which could reach about 94.5% at 1.8°N, while the depletion on 18 August was about 87.8% around 3°N. The movements of the bubbles on 17 August showed to be much faster than those on 18 August. For instance, in meridional direction, the bubble on 17 August moved upward about 600 m/s, while the bubble on 18 August

moved upward with a maximum of about 300 m/s. The movements of bubble in parallel direction on 18 August showed disturbance, some moved southward, other moved northward.

Huang et al. (2014) indicated that plasma could move to a high altitude by the $E \times B$ drift over the magnetic equator and would be driven by the gravitational force to move to higher latitudes along the field lines. As shown in Figure 1, the IMF B_z was about −5 nT (southward), and the IEFs were about 0.85 mV/m at 00 UT and 1.9 mV/m at 01 UT on 18 August, respectively, indicating that even if there were penetration electric field from high latitude, it should have limited effect on the low latitude. The background ionosphere may not be affected significantly by the IEF, leading to the upward movement of the ionosphere. Thus, the high parallel velocities of the particles inside the blobs, recorded by ROCSAT-1 around 0.35 UT on 18 August, may not be contributed to the penetration electric field. Furthermore, in previous reports, the parallel velocity of the plasma inside the blobs was less than 300 m/s (e.g., Haaser et al., 2012; Huang et al., 2014; Klenzing et al., 2011; Le et al., 2003). If only under the effect of the gravitational force, the particles could not move as fast as 480 m/s, which means that there are other factors to drive the particles along the field lines.

It should also be noted that percentage of O^+ inside the blob decreased and H^+ percentage increased, which was similar with the variations inside the plasma depletions shown in Figure 2 and different with the results reported by Yokoyama et al. (2007). The ion temperature inside the bubbles and blobs also increased. It means that the source of the plasma within the blob may be from the higher altitude and the blobs may be related with the bubbles. Moreover, on 17 August, the background density outside the blobs was about 5.47×10^4 cm^{-3} (10^4 order) and the density inside the blobs was about 2.13×10^5 cm^{-3} (10^5 order), while the background density outside the bubbles was about 3.07×10^5 cm^{-3} (10^5 order) and the density inside the bubbles was about 1.68×10^4 cm^{-3} (10^4 order). It is possible that the particles around the bubbles were transported to higher latitude by the meridional wind and accumulated and formed a density enhancement and the bubbles became more depleted, also leading to the percentage of O^+ decreased and H^+ increased in low-latitude region (around 25°N), as shown in Figure 2II. Thus, the blobs recorded on local night of 17 August could be related with the plasma bubbles and the meridional wind.

Unfortunately, there are no direct observations of the meridional wind in the ionosphere; we provide two hypothesis depending on the different wind directions, as shown in Figures 6 and 7, respectively. Similar with the hypothesis of Huang et al. (2014), a schematic illustration of the development of plasma bubbles and blobs under the effect of the meridional (poleward) neutral wind and the polarization electric field is given in Figure 6.

Plasma bubbles are initiated after the sunset at the bottomside *F* region due to the Rayleigh-Taylor instability (Kelley, 2009), and a strong zonal polarization electric field is also generated due to the plasma depletions. As shown in Figure 6a, the bubbles denoted by the green blocks will move upward to the *F* region under the effect of the eastward polarization electric field (upward $E \times B$ drift) and move poleward along the field lines under the effects of the poleward neutral wind. The motion directions of the plasma depend on the magnitude of the electric field and neutral wind, which are represented by the red dashed lines.

With the motion and evolution of the bubbles, the large-scale bubbles may bifurcate and break up into some smaller-scale bubbles, recorded by ROCSAT-1 several hours after sunset, arraying along the field lines. Some plasma particles inside the bubbles will move to higher altitudes and higher latitudes under the effects of the polarization electric field and parallel component of the poleward wind ($U_{//}$), respectively. When the downward gravitational force and wind are balanced by the upward diffusive force in low-latitude region, the particles stop flowing and accumulate to form a density enhancement relative to the background, represented by the red blocks. The density enhancements show some similar characteristics with the bubbles, such as the decrease in the relative concentration of O^+ to H^+ and the increase of ion temperature shown in Figure 2. Due to the interhemispheric poleward wind, denoted by the different lengths in Figure 6, the motions of the particles are different between the two hemispheres. For instance, on 17 August 2003, the wind in the northern hemisphere was stronger than that in the southern hemisphere; the movements of plasma in the northern hemisphere stopped first, and a density enhancement occurred around 16°N, which was detected firstly by GRACE, as shown in Figures 4 and 6b. In southern hemisphere, the particles would keep moving upward and poleward, under the effects of the zonal electric field and weaker poleward wind. The particles stopped the motion at a higher altitude and higher latitude relative to that in northern hemisphere, around −20 to −25°N and formed density enhancements, which were recorded by ROCSAT-1 at 590 km, as shown in

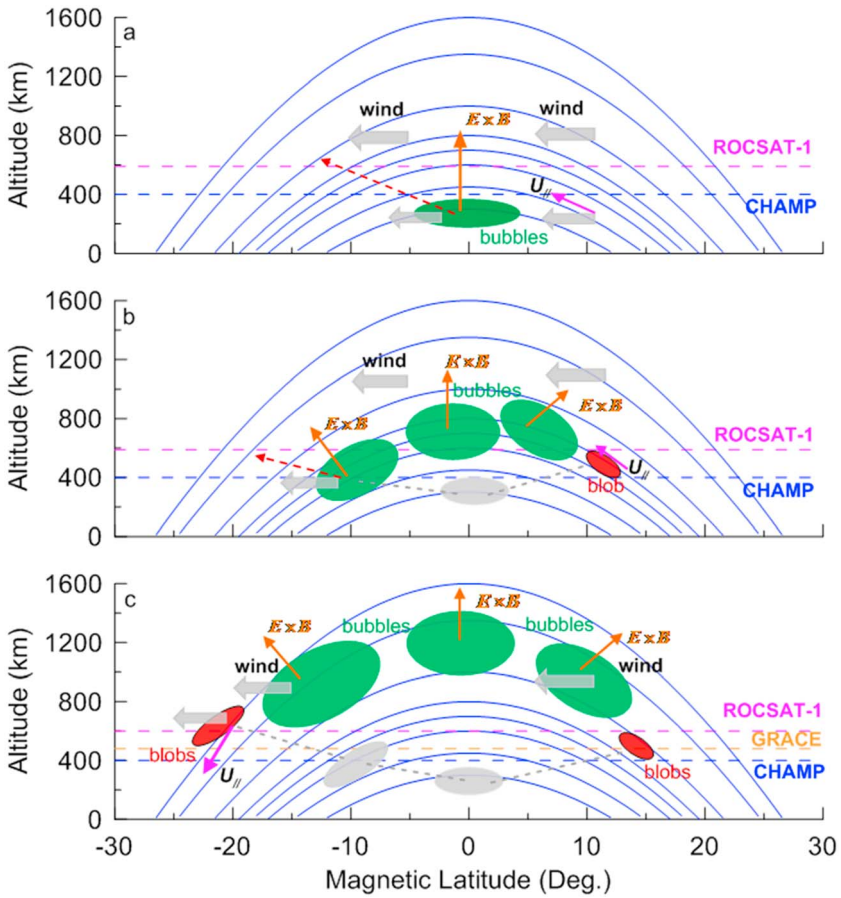

Figure 7. Similar with Figure 6, illustration of the formation of the blobs under the effects of the zonal polarization electric field and transequatorial neutral wind.

Figures 2 and 6c. Due to the effects of the $U_{//}$, the parallel velocity of the particles was accelerated to about 480 m/s. Consequently, the TEC also displayed enhancements in low-latitude regions, as shown in Figure 5. Moreover, the meridional wind is interhemispheric asymmetric, and the effect of the meridional wind on the motion of the particles would be different, leading to the asymmetric performances of the blobs on the two hemispheres.

During the summer solstice, the meridional neutral wind is usual transequatorial and flows from the summer hemisphere to winter hemisphere (Hargreaves, 1992). The effects of transequatorial wind on the formation of plasma blobs are also discussed for the general conditions. Similar with Figure 6, illustration of the development of the plasma bubbles and blobs is given in Figure 7.

Plasma bubbles first occur after the sunset at the bottomside *F* region due to the Rayleigh-Taylor instability (Kelley, 2009); a strong zonal polarization electric field is also generated due to the plasma depletions. In Figure 7a, due to the existence of the zonal electric field and meridional wind, the bubbles will move upward and move poleward, respectively. In the summer (northern) hemisphere, the equatorward wind will raise the plasma particles from the lower altitude and higher latitude to higher altitude and lower latitude, respectively. The bubbles move upward due to the zonal electric field and move poleward along the field lines to higher latitudes due to the gravitational diffusion, respectively. During the passage of the bubbles, the particles from the lower ionosphere are transported to higher altitude along the field lines under the effect of the equatorward wind. The bubbles encounter the particles from the lower ionosphere around the EIA crest, and a balance between the upward forces and the diffusion reaches. Thus, the particles pile up at the side of the EIA crest and form a density enhancement that is detected by the satellite (GRACE), as shown in Figures 4 and 7b. It should be noted that the enhancement is less than that in southern hemisphere because the

plasmas from the lower ionosphere by the equatorward wind neutralize the depletions inside the bubbles at the height.

In winter (southern) hemisphere, the bubbles will move upward and poleward. With the motion and evolution of the bubbles, the large-scale bubbles may bifurcate and break up into some smaller-scale bubbles, arraying along the field lines. Under the effects of the component of poleward neutral wind ($U_{//}$) and zonal polarization electric field, in southern hemisphere, part particles inside the bubbles moved along the field lines to higher latitudes and higher altitudes, respectively. When the downward gravitational force and wind are balanced by the upward diffusive force in low-latitude region, the particles stop flowing and accumulate to form a density enhancement relative to the background, represented by the red blocks. For instance, on 17 August 2003, the particles stopped the motion around −20 to −25°N and formed density enhancements, which were recorded by ROCSAT-1 around 590 km, as shown in Figure 7c. Due to the effects of the $U_{//}$, the parallel velocity of the particles was accelerated to about 480 m/s. Consequently, the TEC also displayed enhancements in low-latitude regions, as shown in Figure 5.

Moreover, the simulations of Krall, Huba, & Martinis (2009) and Krall et al. (2010) reproduced the formation of the blobs under the effects of a mild meridional wind. For instance, in Krall et al. (2010), a northward wind produced a density enhancement at the north of the magnetic equator, which was consistent with the results shown in Figures 2II and 4. The blobs at the south of the magnetic equator were formed under the effects of the southward wind, and the blob at the north of the magnetic equator was formed under the effect of the northward wind. The results all suggest that the effects of meridional wind on the formation of plasma blob should not be neglected.

In general, based on the results shown in Figures 2–5, it suggests that the meridional wind may also have the effects on the formation of plasma blobs, besides the strong zonal polarization electric field resulting from the development of the plasma bubbles proposed by Huang et al. (2014). As proposed by Huang et al. (2014), a polarization electric field generated with the formation of the plasma bubbles, and particles were transported to higher altitudes under the effect of $E \times B$. Under the effects of the gravity, the particles would flow downward along the field line to lower altitudes and higher latitudes and stop flowing in a place when they reach a balance between the gravity and the upward force. Thus, a density enhancement would occur in low-latitude region. In simulations of Krall et al. (2010), the results also indicated that growing bubbles produced upward $E \times B$ drift, moving density upward faster than gravity moves it downward, and resulting in a density enhancement around the crests. Kil et al. (2011) suggested that electric fields and neutral winds could be responsible for the appearance of the enhancements from Communication/Navigation Outage Forecasting System (around 500 km) in their case.

The poleward wind would also cause the EIA to be inhibited and become asymmetric, such that the northern crest was much farther away from the equator shown in Figures 4 and 5.

On 18 August, due to the absence of meridional wind above GRACE altitude, the particles were not transported to higher latitudes and lower altitude from the topside ionosphere; thus, there were no related blobs which may be detected by satellites or recorded by ground-based receivers, such as the observations shown in Figures 3 and 5.

The enhanced meridional wind (poleward) during the storm periods may be linked with the "meteorological processes," arising from the upward propagating gravity waves, tides, and planetary waves (PWs; Lastovicha, 2006).

Large-scale traveling ionospheric disturbances (LSTIDs) during the storm periods are recognized as a manifestation of atmospheric gravity waves in the ionosphere. LSTIDs, which usually propagate equatorward with a period of 0.5–3 hr, may propagate poleward and propagate simultaneously equatorward and poleward (Ding et al., 2013; Habarulema et al., 2015, 2016). During the passage of LSTIDs, the equatorward neutral wind could turn to poleward and the poleward neutral wind could be enhanced (Shiokawa et al., 2003). The velocity of LSTID is usual about 400–1,000 m/s, which may accelerate the parallel velocity of the blob and bubble. Moreover, the large-scale wave structure may also play an important role in the occurrences of equatorial spread *F* (Tsunoda et al., 2010). Thus, LSTIDs may also play an important role in the formation of the blobs during the storms, and the occurrences of the blobs shown in this study may be related with the LSTIDs, not the MSTIDs suggested by Kil et al. (2015).

Though the PWs cannot penetrate directly to ionospheric *F* region, they may also cause the variations of meridional wind in the ionosphere via interaction with the tides or nonlinear processes. The effects of PW on the variability of *F* layer in the ionosphere have been studied by many previous works, which are out of the scope of this study. The most significant effect of the PW on the ionospheric variations is the zonal electric field, relating with the vertical ion drift and the occurrence of the irregularities in low-latitude regions (Abreu et al., 2014). The relationship between the PW and the occurrence of the irregularities should be concerned in future studies.

As mentioned by Huang et al. (2014), the meridional neutral wind is a possible important factor leading to the formation of the blobs, and the mechanisms proposed in the previous studies may also work, such as only the polarization electric field proposed by Huang et al. (2014) and MSTIDs under quiet conditions proposed by Kil et al. (2015). Furthermore, as pointed out by Haaser et al. (2012) and Klenzing et al. (2011), the blobs may generate by different factors or mechanisms under different geophysical conditions, which need to be further studied. For instance, some reports also denoted that the occurrences of the blobs may be not related with the plasma bubbles; the blobs could occur at the absence of the bubbles (Kil et al., 2011, 2015). When the bubbles are absent, the polarization electric field leading to the formation of the density enhancement is not generated. The blobs could not occur following the hypothesis of Huang et al. (2014); the effects of the neutral wind could be considered.

5. Conclusions

The multisatellite observations and IGS TEC map were used to study the possible factors leading to the development of the plasma density enhancements during a storm period. The plasma depletions and enhancements were detected by ROCSAT-1 around 345°E longitude sector at different LT on 17 August, before the midnight after the SSC. The depletions were recorded first around 21.6 LT, while the blobs were detected around 23.3 LT. However, only the depletions were observed on 18 August at the same longitude sector and at nearly the same time as that on 17 August. The movements of the bubbles and blobs displayed different characteristics on 17 August. The blobs in the southern hemisphere moved southward with a speed of about 480 m/s, and the bubbles moved northward in the northern hemisphere at about 200 m/s. The percentage of O^+ decreased and H^+ increased inside the blobs and bubbles, which represent that the blobs were related with the bubbles. On 17 August, a density enhancement about 14.9% at 16.9°N was detected by GRACE, and TEC enhancements in low-latitudinal regions of both hemispheres were also observed. From CHAMP, GRACE observations, and TEC variations in EIA regions, the EIA was inhibited and displayed more asymmetric on 17 August, which can be attributed to the meridional wind, and became stronger on 18 August. Combining the characteristics of plasma velocities and the composition variations inside the blobs and bubbles with the results from CHAMP, GRACE, and TEC variations suggests that the meridional wind is crucial and plays an important role in the development of the plasma blobs. The poleward neutral wind would transport the particles around the equatorial plasma depletions to higher latitudes along the field lines. When reaching a balance between the downward force and the upward diffusive force, the particles stop movements and accumulate in low-latitude regions, resulting in formation of density enhancements which may be recorded by the satellites and ground-based receivers.

The meridional wind during the disturbed periods may be linked with the LSTIDs, which propagated poleward. During the passage of the LSTIDs, the poleward neutral winds were enhanced, leading to the parallel movements of the particles along the field lines. It is suggested that the LSTIDs are related with the occurrence of the plasma blobs during the disturbance. The relationship between the occurrence of the blobs and the LSTIDs and other factors (such as PWs) need to be further studied in the future.

Acknowledgments
This work is supported by the National Natural Science Foundation of China (41474134, 41474135, and 41704161). The author Weihua Luo thanks Prof. Jisheng Xu for useful discussions. The SYM-H data were obtained from the World Data Center (WDC) in Kyoto. We acknowledge UCAR, NCU, and the ACE science centre for providing the satellites data, respectively. The CHAMP and GRACE data were downloaded from CDAAC (http://cdaac-www.cosmic.ucar.edu/cdaac/products.html). The ROCSAT-1 data were downloaded from NCU (http://sdbweb.ss.ncu.edu.tw/ipei_download.html). The IMF and solar wind speed are downloaded from the ACE center (http://www.srl.caltech.edu/ACE/ASC/). The IGS TEC data were downloaded from the Madrigal Database at Haystack Observatory (http://madrigal.haystack.mit.edu/madrigal/index.html). The authors are grateful to the reviewers and editors for their constructive comments on the manuscript.

References

Abreu, A. J., Fagundes, P. R., Bolzan, M. J. A., Gende, M., Brunini, C., Jesus, R., et al. (2014). Traveling planetary wave ionospheric disturbances and their role in the generation of equatorial spread F and GPS phase fluctuations during the last extreme low solar activity and comparison with high solar activity. *Journal of Atmospheric and Solar-Terrestrial Physics*, *117*, 7–19. https://doi.org/10.1016/j.jastp.2014.05.005

Aydogdu, M. (1988). North-south asymmetry in the ionospheric equatorial anomaly in the African and the West Asian regions produced by asymmetrical thermospheric winds. *Journal of Atmospheric and Terrestrial Physics*, *50*(7), 623–627. https://doi.org/10.1016/0021-9169(88)90060-8

Balan, N., Souza, J., & Bailey, G. J. (2018). Recent developments in the understanding of equatorial ionization anomaly: A review. *Journal of Atmospheric and Solar-Terrestrial Physics*, *171*, 3–11. https://doi.org/10.1016/j.jastp.2017.06.020

Choi, H. S., Kil, H., Kwak, Y. S., Park, Y. D., & Cho, K. S. (2012). Comparison of the bubble and blob distribution during the solar minimum. *Journal of Geophysical Research*, *117*, A04314. https://doi.org/10.1029/2011JA017292

Dashora, N., & Pandey, R. (2005). Observations in equatorial anomaly region of total electron content enhancements and depletions. *Annales de Geophysique*, *23*(7), 2449–2456. https://doi.org/10.5194/angeo-23-2449-2005

Ding, F., Wan, W., Ning, B., Zhao, B., Lin, Q., Wang, Y., et al. (2013). Observations of poleward-propagating large-scale traveling ionospheric disturbances in southern China. *Annales de Geophysique*, *31*(2), 377–385. https://doi.org/10.5194/angeo-31-377-2013

Haaser, R. A., Earle, G. D., Heelis, R. A., Klenzing, J., Stoneback, R., Coley, W. R., & Burrell, A. G. (2012). Characteristics of low-latitude ionospheric depletions and enhancements during solar minimum. *Journal of Geophysical Research*, *117*, A10305. https://doi.org/10.1029/2012JA017814

Habarulema, J. B., Katamzi, Z. T., & Yizengaw, E. (2015). First observations of poleward large-scale traveling ionospheric disturbances over the African sector during geomagnetic storm conditions. *Journal of Geophysical Research: Space Physics*, *120*, 6914–6929. https://doi.org/10.1002/2015JA021066

Habarulema, J. B., Katamzi, Z. T., Yizengaw, E., Yamazaki, Y., & Seemala, G. (2016). Simultaneous storm time equatorward and poleward large-scale TIDs on a global scale. *Geophysical Research Letters*, *43*, 6678–6686. https://doi.org/10.1002/2016GL069740

Hargreaves, J. K. (1992). *The solar-terrestrial environment*. Cambridge: Cambridge University Press. ISBN: 0-521-32748-2.

Huang, C. S., Le, G., de La Beaujardiere, P. A., Roddy, D. E., Hunton, R. F. P., & Hairston, M. R. (2014). Relationship between plasma bubbles and density enhancements: Observations and interpretation. *Journal of Geophysical Research: Space Physics*, *119*, 1325–1336. https://doi.org/10.1002/2013JA019579

Kelley, M. C. (2009). *The Earth's ionosphere: Plasma physics & electrodynamics*, *International geophysics series* (2nd ed.). San Diego, CA: Academic. ISBN: 978–0–12-088425-4.

Kil, H., Choi, H. S., Heelis, R. A., Paxton, L. J., Coley, W. R., & Miller, E. S. (2011). Onset condition of bubbles and blobs: A case study on 2 March 2009. *Geophysical Research Letters*, *38*, L06101. https://doi.org/10.1029/2011GL046885

Kil, H., Kwak, Y. S., Lee, W. K., Miller, E. S., Oh, S. J., & Choi, H. S. (2015). The causal relationship between plasma bubbles and blobs in the low-latitude F region during a solar minimum. *Journal of Geophysical Research: Space Physics*, *120*, 3961–3969. https://doi.org/10.1002/2014JA020847

Klenzing, J. H., Rowland, D. E., Pfaff, R. F., Le, G., Freudenreich, H., Haaser, R. A., et al. (2011). Observations of low-latitude plasma density enhancements and their associated with plasma drifts. *Journal of Geophysical Research*, *116*, A09324. https://doi.org/10.1029/2011JA016711

Krall, J., Huba, J. D., Joyce, G., & Yokoyama, T. (2010). Density enhancements associated with equatorial spread F. *Annales de Geophysique*, *28*(2), 327–337. https://doi.org/10.5194/angeo-28-327-2010

Krall, J., Huba, J. D., Joyce, G., & Zalesak, S. T. (2009). Three-dimensional simulation of equatorial spread-F with meridional wind effects. *Annales de Geophysique*, *27*(5), 1821–1830. https://doi.org/10.5194/angeo-27-1821-2009

Krall, J., Huba, J. D., & Martinis, C. R. (2009). Three-dimensional modeling of equatorial spread F airglow enhancements. *Geophysical Research Letters*, *36*, L10103. https://doi.org/10.1029/2009GL038441

Lastovicha, J. (2006). Forcing of the ionosphere by waves from below. *Journal of Atmospheric and Solar-Terrestrial Physics*, *68*(3-5), 479–497. https://doi.org/10.1016/j.jastp.2005.01.018

Le, G., Huang, C. S., Pfaff, R. F., Su, S. Y., Yeh, H. C., Heelis, R. A., et al. (2003). Plasma density enhancements associated with equatorial spread F: ROCSAT-1 and DMSP observations. *Journal of Geophysical Research: Space Physics*, *108*(A8), 1318. https://doi.org/10.1029/2002JA009592

Lin, C. H., Richmond, A. D., Heelis, R. A., Bailey, G. J., Lu, G., Liu, J. Y., et al. (2005). Theoretical study of the low- and midlatitude ionospheric electron density enhancement during the October 2003 superstorm: Relative importance of the neutral wind and the electric field. *Journal of Geophysical Research*, *110*, A12312. https://doi.org/10.1029/2005JA011304

Martinis, C., Baumgardner, J., Mendillo, M., Su, S. Y., & Aponte, N. (2009). Brightening of 630.0 nm equatorial spread-F airglow depletions. *Journal of Geophysical Research*, *114*, A06318. https://doi.org/10.1029/2008JA013931

Maruyama, T. (1988). A diagnostic model for equatorial spread-F 1. Model description andapplication to electric field and neutral wind effects. *Journal of Geophysical Research*, *93*, 14,611–14,622. https://doi.org/10.1029/JA093iA12p14611

Maruyama, T., Saito, S., Kawamura, M., Nozaki, K., Krall, J., & Huba, J. D. (2009). Equinoctial asymmetry of a low-latitude ionosphere-thermosphere system and equatorial irregularities: Evidence for meridional wind control. *Annales de Geophysique*, *27*(5), 2027–2034. https://doi.org/10.5194/angeo-27-2027-2009

McNamara, L., Cooke, D. L., Valladares, C. E., & Reinisch, B. W. (2007). Comparison of CHAMP and Digisonde plasma frequencies at Jicamarca, Peru. *Radio Science*, *42*, RS2005. https://doi.org/10.1029/2006RS003491

Oya, H., Takahashi, T., & Watanabe, S. (1986). Observation of low latitude ionosphere by the impedance probe on board the Hinotori satellite. *Journal of Geomagnetism and Geoelectricity*, *38*(2), 111–123. https://doi.org/10.5636/jgg.38.111

Park, J., Min, K. W., Kim, V. P., Kil, H., Kim, H. J., Lee, J. J., et al. (2008). Statistical description of low-latitude plasma blobs as observed by DMSP F15 and KOMPSAT-1. *Advances in Space Research*, *41*(4), 650–654. https://doi.org/10.1016/j.asr.2007.04.089

Park, J., Min, K. W., Lee, J. J., Kil, H., Kim, V. P., Kim, H. J., et al. (2003). Plasma blob events observed by KOMPSAT-1 and DMSP F15 in the low latitude nighttime upper ionosphere. *Geophysical Research Letters*, *30*(21), 2114. https://doi.org/10.1029/2003GL018249

Pimenta, A. A., Sahai, Y., Bittencourt, J. A., Abdu, M. A., Takahashi, H., & Taylor, M. J. (2004). Plasma blobs observed by ground-based optical and radio techniques in the Brazilian tropical sector. *Geophysical Research Letters*, *31*, L12810. https://doi.org/10.1029/2004GL020233

Pimenta, A. A., Sahai, Y., Bittencourt, J. A., & Rich, F. J. (2007). Ionospheric plasma blobs observed by OI630 nm all-sky imaging in the Brazilian tropical sector during the major geomagnetic storm of April 6–7, 2000. *Geophysical Research Letters*, *34*, L02820. https://doi.org/10.1029/2006GL028529

Shiokawa, K., Otsuka, Y., Ogawa, T., Kawamura, S., Yamamoto, M., Fukao, S., et al. (2003). Thermospheric wind during a storm-time large-scale traveling ionospheric disturbance. *Journal of Geophysical Research*, *108*(A12), 1423. https://doi.org/10.1029/2003JA010001

Tapley, B. D., Bettadpur, S., Watkins, M., & Reigber, C. (2004). The Gravity Recovery and Climate Experiment: Mission overview and early results. *Geophysical Research Letters*, *31*, L09607. https://doi.org/10.1029/2004GL019920

Tsunoda, R. T., Bubenik, D. M., Thampi, S. W., & Yamamoto, M. (2010). On large-scale wave structure and equatorial spread F without a post-sunset rise of the F layer. *Geophysical Research Letters*, *37*, L07105. https://doi.org/10.1029/2009GL042357

Walker, G. O. (1981). Longitudinal structure of the equatorial ionization anomaly: A review. *Journal of Atmospheric and Terrestrial Physics*, *43*(8), 763–774. https://doi.org/10.1016/0021-9169(81)90052-0

Watanabe, S., & Oya, H. (1986). Occurrence characteristics of low latitude ionosphere irregularities observed by impendence probe on board the Hinotori satellite. *Journal of Geomagnetism and Geoelectricity*, *38*(2), 125–149. https://doi.org/10.5636/jgg.38.125

Xiong, C., Lühr, H., & Fejer, B. G. (2015). Validation of GRACE electron densities by incoherent scatter radar data and estimation of plasma scale height in the topside ionosphere. *Advances in Space Research*, *55*(8), 2048–2057. https://doi.org/10.1016/j.asr.2014.07.022

Xiong, C., Park, J., Luhr, H., Stolle, C., & Ma, S. Y. (2010). Comparing plasma bubble occurrence rates at CHAMP and GRACE altitudes during high and low solar activity. *Annales de Geophysique*, *28*(9), 1647–1658. https://doi.org/10.5194/angeo-28-1647-2010

Yeh, H. C., Su, S. Y., Yeh, Y. C., Wu, J. M., Heelis, R. A., & Holt, B. J. (1999). Scientific mission of the IPEI payload onboard ROCSAT-1. *Terrestrial, Atmospheric and Oceanic Sciences*, *10*(1–1), 019–042. https://doi.org/10.3319/TAO.1999.10.S.19(ROCSAT)

Yokoyama, T., Su, S. Y., & Fukao, S. (2007). Plasma blobs and irregularities concurrently observed by ROCSAT-1 and equatorial atmosphere radar. *Journal of Geophysical Research*, *112*, A05311. https://doi.org/10.1029/2006JA012044